batteries

MDPI

Article

Evaluating the Role of Entropy Change in Lithium-Ion Battery Electro-Thermal Modelling

Félix-Antoine LeBel [1,2], Pascal Messier [1,2], Mathieu Blanchard [2] and João Pedro F. Trovão [1,3,4,*]

[1] electric-Transport, Energy Storage and Conversion (e-TESC) Lab., Université de Sherbrooke, Sherbrooke, QC J1K 2R1, Canada; felix-antoine.lebel@usherbrooke.ca (F.-A.L.); pascal.messier@usherbrooke.ca (P.M.)
[2] SysNergie Inc., Sherbrooke, QC J1N 0G2, Canada; mathieu.blanchard@sysnergie.ca
[3] Institute for Systems Engineering and Computers at Coimbra (INESC Coimbra), Department of Electrical and Computer Engineering, University of Coimbra, Polo II, 3030-290 Coimbra, Portugal
[4] Coimbra Institute of Engineering, Polytechnic of Coimbra (IPC-ISEC), 3030-199 Coimbra, Portugal
* Correspondence: joao.trovao@usherbrooke.ca

Abstract: The accurate estimation of lithium-ion cell internal temperature is crucial for the safe operation of battery packs, especially during high discharge rates, as operating outside the safe temperature range can lead to accelerated degradation or catastrophic failures. Heat generation in lithium-ion cells arises primarily from ohmic losses and entropy change (ΔS), yet the latter remains frequently overlooked in battery modelling. However, the impact of considering or discarding ΔS from electro-thermal modelling remains subject to debate. This research highlights the critical role of ΔS in improving the accuracy of electro-thermal models for lithium-ion batteries, particularly in high-fidelity thermal simulations. It presents a systematic integration, ΔS, into electro-thermal models, leveraging the energetic macroscopic representation (EMR) approach to enhance predictive accuracy, a methodology not previously structured in this manner. This paper addresses this issue by performing a comparative analysis of an electro-thermal model (ETM) with and without ΔS. The findings provide clear insights into the role of entropy in electro-thermal modelling, demonstrating that while entropy change has a minimal impact on electrical behaviour prediction, it plays a crucial role in accurately capturing temperature dynamics, helping define the conditions under which it must be considered in simulations. While entropy can be neglected for coarse heat generation estimation, its inclusion enhances temperature prediction accuracy by up to 4 °C, making it essential for applications requiring precise thermal management. This study offers a detailed analysis of the conditions under which ΔS becomes critical to model accuracy, providing actionable guidance for battery engineers and researchers.

Keywords: lithium-ion battery; heat generation; entropic coefficient; electro-thermal model; electric equivalent circuit

check for updates

Academic Editors: Chris Mi, Zhi Cao and Naser Vosoughi Kurdkandi

Received: 11 January 2025
Revised: 10 February 2025
Accepted: 14 February 2025
Published: 20 February 2025

Citation: LeBel, F.-A.; Messier, P.; Blanchard, M.; Trovão, J.P.F. Evaluating the Role of Entropy Change in Lithium-Ion Battery Electro-Thermal Modelling. *Batteries* **2025**, *11*, 84. https://doi.org/10.3390/batteries11030084

Copyright: © 2025 by the authors. Licensee MDPI, Basel, Switzerland. This article is an open access article distributed under the terms and conditions of the Creative Commons Attribution (CC BY) license (https://creativecommons.org/licenses/by/4.0/).

1. Introduction

Lithium-ion batteries (LIBs) are widely used across various applications, from electric vehicles (EVs) to battery energy storage systems (BESS), where safety, durability, and reliability are of paramount concern. Temperature is a critical factor influencing the performance and longevity of LIBs. Temperature directly influences key parameters such as cell impedance, capacity retention, and permissible charge/discharge rates. Furthermore, temperature accelerates the degradation of electrode materials, a process known as aging. Several recent events have highlighted the dramatic consequences of the violent

catastrophic failure of LIBs. Excessive heat buildup is a known failure causing thermal runaway (TRA), posing significant safety risks [1].

To ensure the safe and reliable operation of LIBs, it is essential to maintain temperature and voltage within specified safe operational windows. The accurate assessment of temperature dynamics and heat generation across diverse operating scenarios by the battery management system (BMS) is crucial for preventing accelerated degradation or TRA [2]. Accurate thermal estimation is particularly vital in the battery pack design phase, influencing both thermal management strategies and overall system design.

Unlike other types of electrical components, LIBs are non-linear electrochemical systems in which heat generation cannot be directly inferred from the nominal internal resistance value. Their behaviour and properties are simultaneously influenced by temperature, the state of charge (SOC), and aging, all of which interact in complex ways. Additionally, structural changes caused by the intercalation and de-intercalation of lithium ions in the electrodes during charge and discharge cycles, in turn causing changes in entropy and enthalpy that alter both the thermal and electrical properties of the cells. The phenomena has been studied by [3], and it has been found that the thermodynamics of lithium intercalation into graphite is governed by a complex interplay of mixing entropy, vibrational entropy, and lithium–lithium interactions.

In lithium-ion batteries, entropy (S) and entropy change (ΔS) are related concepts, but they represent different aspects of the thermodynamics within the battery system. Entropy in the context of a lithium-ion battery refers to the inherent thermodynamic property that quantifies the degree of disorder or randomness of the battery's system in a specific state. Each component and phase of a lithium-ion battery—such as the cathode, anode, and electrolyte—has a certain entropy value based on its structure and composition. In general, higher entropy signifies a greater degree of disorder.

Entropy change (ΔS) is a dynamic concept that measures the difference in entropy between two states, particularly during chemical reactions or physical processes, like charging and discharging. For LIBs, this is especially relevant because entropy change can reveal valuable insights into electrochemical processes, like lithium-ion intercalation and de-intercalation. Entropy change is often calculated for reactions occurring at the electrodes and can provide information on the energy efficiency and temperature dependence of the battery's operation. Entropy is a static property of a given state, while entropy change is dynamic, reflecting the shift between two states (e.g., before and after lithium-ion intercalation).

Entropy change impacts thermal management in lithium-ion batteries. During charging and discharging, changes in entropy contribute to heat generation within the battery. Understanding these entropy changes is crucial in designing systems to manage temperature and avoid overheating. Entropy changes can be experimentally measured through thermodynamic methods and provide insights into how temperature affects the electrochemical potential of the battery, which is useful for optimizing operating conditions.

Since the characterization of ΔS is a long and tedious process, it is often overlooked in system-level models, such as electric vehicle simulation. Omitting this fundamental behaviour can potentially lead to discrepancies between measurements and model predictions. This paper investigates whether accounting for entropy change can improve the accuracy of heat generation and temperature estimations in lightweight electro-thermal models used in the BMS and system-level performance assessement.

Estimating the various states of an LIB is a critical function of modern BMSs and a key consideration in LIB design. Contemporary modelling approaches differ in complexity, with the choice of model depending on the desired balance between accuracy, spatial resolution, and computational feasibility.

Physics-based models (PBMs) are designed to improve the accuracy of battery modelling by capturing detailed internal dynamics. The foundation of fully physics-based lithium-ion battery models is the pseudo-two-dimensional (P2D) porous electrode model, also known as the Doyle–Fuller–Newman model, named after the researchers who pioneered its development [4–6]. This model is based on porous electrode theory, concentrated solution theory, and the Butler–Volmer kinetic equations.

Variants of the P2D model include the single-particle model (SPM) [7], which simplifies calculations to reduce computational demands for embedded applications, and the multi-dimensional multi-physics model (MuDiMod) [8,9], which increases model complexity to investigate the intricate internal behaviour of lithium-ion cells. PBMs offer insights into internal battery processes such as lithium-ion diffusion, Ohmic effects, and electrochemical kinetics. These models enable the exploration of battery degradation mechanisms, the prediction of the SOC and state of health (SOH) with aging considerations, and the development of optimal charging strategies. However, PBMs are composed of numerous partial differential equations (PDEs), requiring significant computational power to solve. This inherent complexity makes the real-time integration of PBMs into low-power controllers found in BMSs impractical [10].

Equivalent-circuit models (ECMs) [11–17] represent LIBs as networks of electronic components such as resistors and capacitors. These resistor–capacitor networks are used to capture battery behaviour over various time constants associated with diffusion and charge-transfer processes [18]. ECMs are based on empirical insights and experimental data, making them the predominant model for real-time SOC estimation in electric vehicle BMSs. Their popularity stems from their ability to predict electrical behaviour quickly and with minimal computational load, as most information can be pre-computed and stored in lookup tables.

Two main methods are commonly used to determine ECM parameters: electrochemical impedance spectroscopy (EIS) [19,20] and the galvanostatic intermittent titration technique (GITT) [21], also known as pulse testing and referred to by various names in the prior literature [22]. ECMs, however, typically do not account for temperature and heat generation effects, so they are often coupled with thermal models of varying complexity to address these factors.

Entropy change (ΔS) represents the heat absorbed or released due to microstructural changes during lithium intercalation. This reversible heat, which differs from non-reversible heat generation related to impedance, is traditionally measured using potentiometric methods [23–25]. However, these measurements are labour-intensive, prompting a common practice of excluding ΔS in the practical thermal modelling of lithium-ion batteries [26].

Neglecting ΔS is a common engineering practice in the thermal modelling of lithium-ion cells. For instance, the models found in [26] all neglect entropy. Ye et al. argued that there is a reversible heat source during discharge at higher currents, thus concluding that entropy can be neglected in such cases [27].

As battery materials evolve to minimize Ohmic losses and new chemistries are developed, the consideration of ΔS could become increasingly relevant to improve model accuracy. This paper aims to offer battery engineers a nuanced perspective on when and to what extent ΔS should be incorporated into electro-thermal models, considering its impact on model accuracy under different operational scenarios.

2. Methodology

In this study, a rigorous methodology was employed to investigate the impact of entropy change. Firstly, a comprehensive model was constructed using MatLab/Simulink, providing a computational framework for analysis. Subsequently, the model's parameters,

crucial for accurate simulation, were determined through various experimental methods. Parameters such as impedance, open-circuit voltage, the coefficient of convection, and entropy change were precisely quantified. To validate fidelity and predictive capability, the model was benchmarked against real-world data obtained from continuous discharge and actual driving cycles. The accuracy of the proposed model was evaluated under constant current discharge and dynamic profile scenarios, offering valuable insights into the importance of considering ΔS. Finally, leveraging the validated model, simulations were conducted to explore various scenarios of continuous currents and power discharge at different rates. The insights obtained from these simulations are intended to help guide engineers in their decision process of whether to include entropy change or not in simulations.

The experimental setup used for this work is pictured in Figure 1. Cells were held in place and connected by ZKE Battery Rack cell fixtures, which had independent probes for voltage measurement and current carrying [28]. Each cell holder was connected to one of the 48 channels of an LBT-2000 (Arbin Instruments, College Station, TX, USA) cell cycler with the four-wire Kelvin method [29]. The precision of each channel was 0.5 mV. This equipment is well suited for detailed battery characterization and Coulombic efficiency studies due to its very high level of precision. The sampling rate of the channels was set to 10 Hz. Throughout all tests, constant ambient temperature in the samples was ensured by placing the samples inside a CSZ MicroClimate (Cincinnati Sub-Zero, Cincinnati, OH, USA) test chamber [30]. The temperature of each cell was measured with Type-T thermocouples, placed midway along the length of the cells, held in place with a thin polyamide film tape.

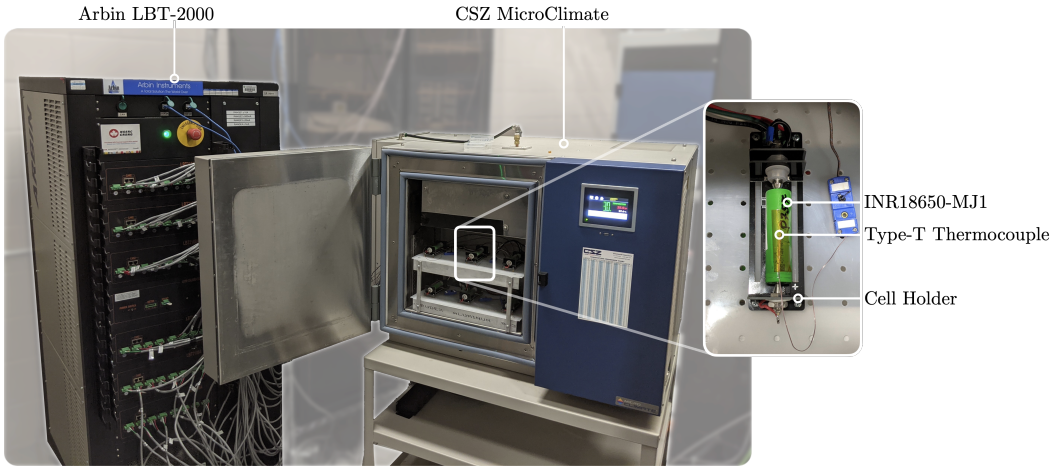


Figure 1. Experimental setup.

For this work, 3.5 Ah INR18650-MJ1 (LG Chem, Seoul, South Korea) cells composed of a nickel–manganese–cobalt cathode and silicon–graphite anode were used. The choice of the INR18650-MJ1 was based on the fact that its behaviour and construction has already been studied in the prior literature [31–38], so it can be tied to several other publications.

The model developed in this work was composed of a lumped thermal model with convection and a first-order RC ECM electrical model. Figure 2 shows the basic representation of the thermal and electrical models. The sign convention used in this work was such that positive current was considered flowing out of the cell to provide power to the load it was connected to.

It was assumed that properties and behaviour were homogeneous throughout the cell body and electrodes. The electrical boundary of the system was the load, and the thermal boundary was natural convection with the surrounding air. The coupling of the two models forming the electro-thermal model (ETM) could be visualized conceptually using energetic macroscopic representation (EMR). Figure 3 illustrates the interactions between the various

physical behaviours within a lithium-ion cell. Similar representations have been depicted in prior work [39].

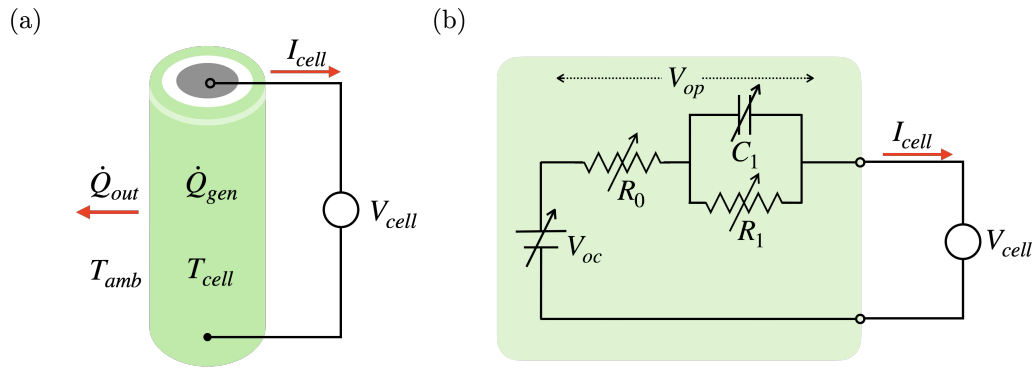


Figure 2. Schematic representation of lithium-ion cell. (**a**) Thermal. (**b**) Electrical.

EMR is a systemic representation for modelling multi-physical systems. It is a well-suited representation for structuring models in a graphical programming environment such as MatLab/Simulink. The model was implemented in MatLab/Simulink R2021b.

In this representation, the behaviour of the cell is broken down in three main components: the electrochemical energy source (designated as Electrodes), the losses (depicted as a multi-physics coupling block), and the thermal inertia. A load model and a thermal boundary conditions model (designated as Load/Supply and Air) complete the ETM. In the model, the electrochemical energy source defines the open-circuit potential of the cell V_0. It is assumed that V_0 is the theoretical voltage of the cell without any current flowing through the cell. The value of V_0 was measured in prior work [22] at temperatures, T, ranging from −20 °C to 60 °C, at increments of 1% SOC, as shown in Figure 4. Its value was estimated by bilinear interpolation within the empirical response surface.

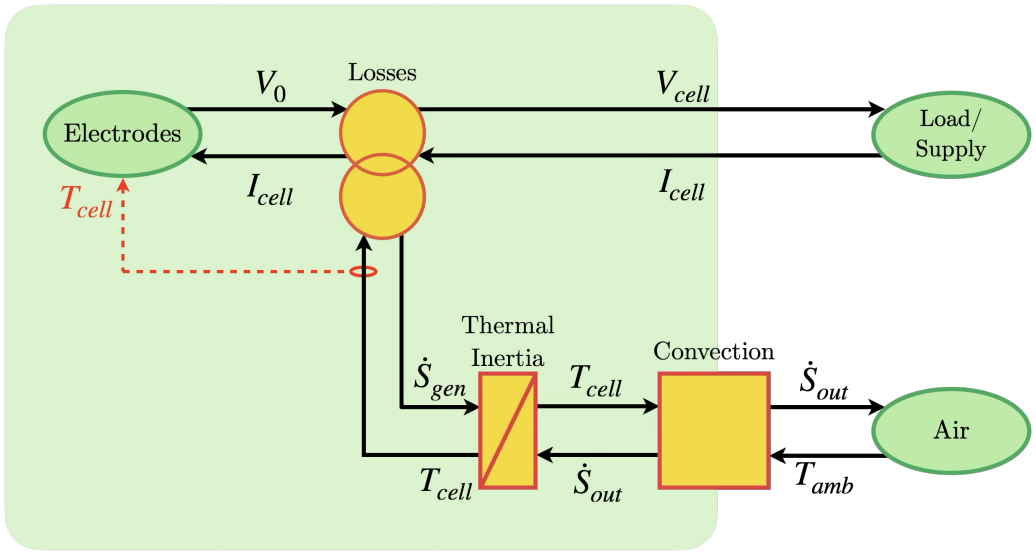


Figure 3. Equivalent energetic macroscopic representation (EMR) of lithium-ion cell.

The electrochemical potential V_0 of a cell is a function of the amount of lithium ions present in the electrodes, or SOC. As ions are intercalated in the anode and cathode, the resulting potential varies accordingly. While the evolution of potential with regard to the degree of lithiation is somewhat linear, phase changes in the microstructure of the electrodes may cause fluctuations to the slope at certain specific SOCs [40]. Note that V_{cell} and V_{op} are functions of the cells SOC θ, temperature T_{cell}, current I_{cell}, and time t, while V_0 is not influenced by the current and time. SOC, θ, is defined as the ratio of the remaining

quantity of electrical charges within the electrodes to the theoretical total amount of useful charges of said electrodes C_0 at the reference temperature (25 °C). The remaining quantity of charges can be computed by the integration of I_{cell} over t. For (1) to be computed correctly, C_0 is expressed in Coulombs (C).

$$\theta = \frac{\int I_{cell} dt}{C_0} \tag{1}$$

A first-order ECM is used to represent overpotentials in this work. The overpotential voltage of a resistor–capacitor (RC) ECM is given in (2) in the general form where the electrical network is composed of the entirely resistive component R_0 and n RC couples, designated by R_k and C_k, where k is the couple instance subscript.

$$V_{op}(\theta, T, t) = R_0(\theta, T)I(t) + \sum_{k=1}^{n} R_k(\theta, T)I(t)e^{-t/R_k(\theta,T)C_k(\theta,T)} \tag{2}$$

This translates to the following transfer function in the Laplace domain (3).

$$V_{op}(\theta, T) = IR_0(\theta, T) + I\sum_{k=1}^{n} \frac{R_k(\theta, T)}{R_k(\theta, T)C_k(\theta, T)s + 1} \tag{3}$$

In the model, V_{cell} is the difference between the potential and overpotential V_{op} caused by the inefficiencies of the various processes (4).

$$V_{\text{cell}}(\theta, T, I, t) = V_{oc}(\theta, T) - V_{\text{op}}(\theta, T, I, t) \tag{4}$$

The effective electrical power of the cell, P_{cell}, is the product of the electrical current I_{cell} and cell voltage V_{cell} (5).

$$P_{\text{cell}} = V_{\text{cell}} I_{\text{cell}} \tag{5}$$

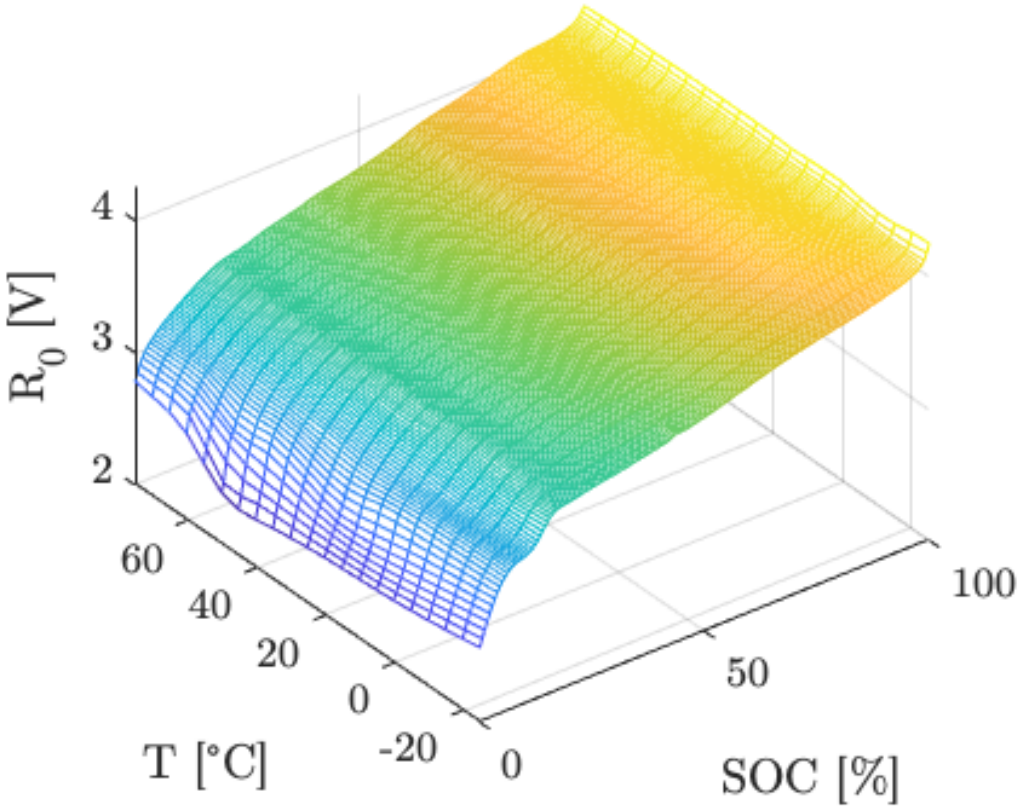


Figure 4. Open-circuit voltage interpolation table.

The complexity of the non-linear property changes with regard to θ and T can be difficult to model. Therefore, empirical mapping as described in [22] remains an accurate and straight-forward approach. Figure 5 shows the response surface for the different impedance parameters of the model. Impedance characteristics are unique to each lithium-ion cell model and manufacturer. They are influenced by factors such as the chemical composition of the electrode's active materials, as well as numerous design- and production-induced parameters, including electrode thickness and particle size [41].

Irreversible losses generated by overpotential (Q_{op}) can be expressed by (6)

$$\dot{Q}_{op} = V_{op} I_{cell} \tag{6}$$

However, the total heat generation inside the cell ($\dot{Q}_{gen}$) is equal to the sum of irreversible losses, $\dot{Q}_{op}$, and reversible losses from entropy change, $\dot{Q}_{ent}$. While ΔS can be seen as a variation in temperature caused by a change in potential, the opposite is also true. Equation (7) describes this relationship, where F is the Faraday constant. Therefore, using the direct correlation between temperature change and voltage change, one can obtain the entropic coefficient of a cell by applying a temperature change to a cell, while measuring the resulting voltage change. This method is known as the potentiostatic method [23–25].

$$\Delta S = F \frac{dV}{dT} \tag{7}$$

In a controlled temperature chamber, T_{cell} was changed from 20 °C to 40 °C with an acclimatization period of approximately 30 min after each temperature change to allow the full entropic phase transformation. Using the experimental setup described earlier, two samples were tested along the entire capacity by discharging the cell at a rate of C/10 and resting at equally spaced intervals of 5% SOCs to perform the test. A similar methodology was proposed by Geifes et al. [42].

This property is dependent of the degree of lithiation of the electrodes or θ at the cell level and has been shown to be independent of the temperatures at which it is measured [25,43]. The entropy change coefficient ΔS is shown in Figure 6.

Assuming linear interpolation between the measurement points, reversible heat flow due to ΔS was computed with Equation (8).

$$\dot{Q}_{\text{ent}} = \frac{-I T_{\text{cell}} \Delta S}{F} \tag{8}$$

The thermal output of the multi-physics losses model was as is stated in (9).

$$\dot{Q}_{\text{gen}} = \dot{Q}_{\text{op}} + \dot{Q}_{\text{ent}} \tag{9}$$

However, as discussed in German et al. [39], losses must be expressed in the flow of entropy as defined by (10) to respect the principles of EMR.

$$\dot{S} = \frac{\dot{Q}}{T} \tag{10}$$

Therefore, (9) becomes (11).

$$\dot{S}_{gen} = \frac{\dot{Q}_{gen}}{T_{cell}} \tag{11}$$

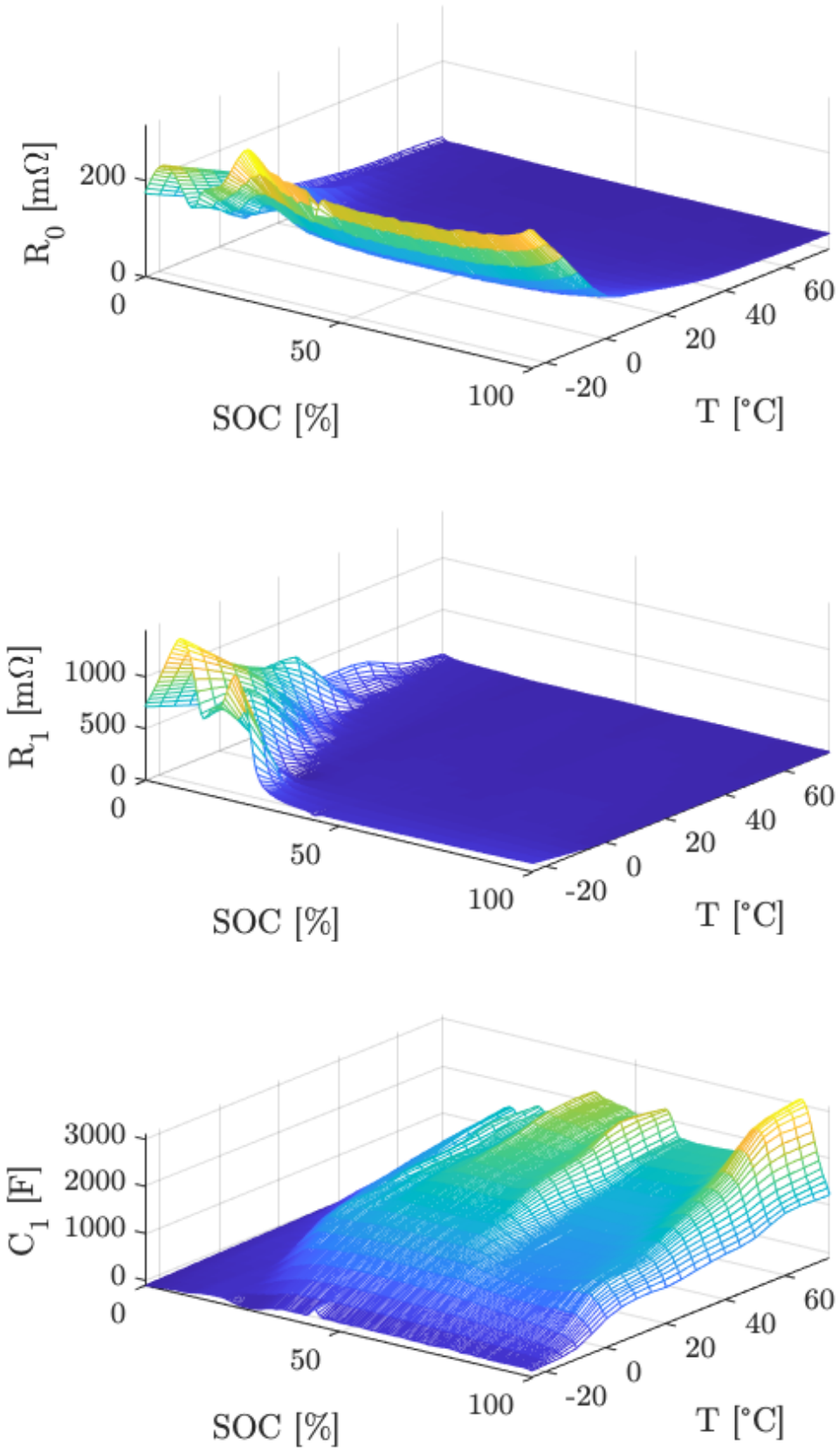


Figure 5. Map of parameters of electrical model.

This result was then fed as an input of the thermal inertia model (Thermal Inertia block in Figure 3). Unless the cell was placed in perfectly adiabatic boundary conditions, heat would leak out of the cell to its surroundings through radiative, convective, and conductive

heat transfer. Radiation losses ($\dot{Q}_{rad}$) were considered negligible under normal operation. Conduction heat losses ($\dot{Q}_{cond}$) were also neglected from this work. Only convection heat transfer ($\dot{Q}_{conv}$) to the surrounding air was considered. To respect EMR formalism, convection heat transfer was expressed as entropy flow, S_{conv}. It was computed by (12).

$$\dot{S}_{\text{conv}} = \frac{hA(T_{\text{cell}} - T_{\text{amb}})}{T_{\text{cell}}} \tag{12}$$

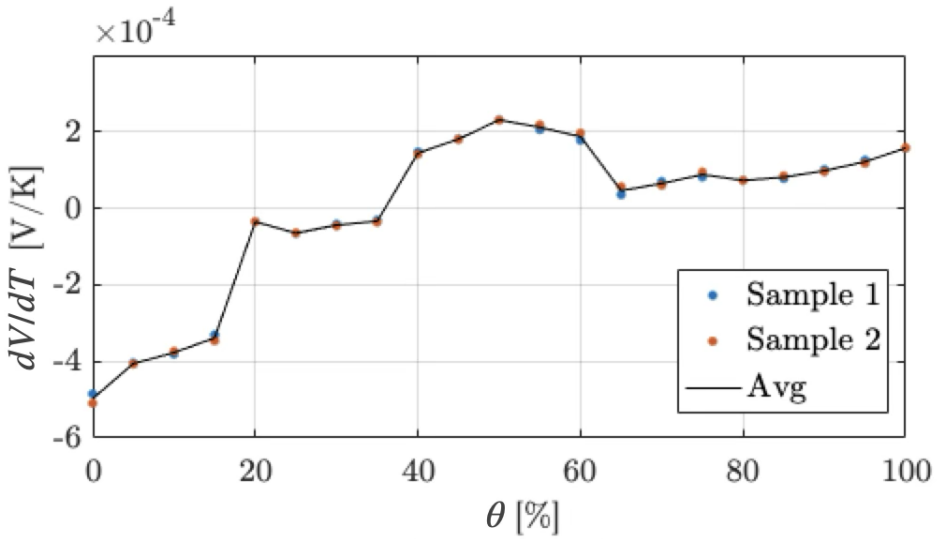


Figure 6. Entropic coefficient of cell at different states of charge.

While the surface area of a cell (A) can be estimated from geometry, the convection coefficient (h) is typically determined experimentally. Its value depends on various parameters such as fluid viscosity, surface finish, object shape, and orientation. The total entropy flow to the environment is given by (13).

$$\dot{S}_{\text{out}} = \dot{S}_{\text{rad}} + \dot{S}_{\text{cond}} + \dot{S}_{\text{conv}} \tag{13}$$

Cell temperature for the next iteration step T^*_{cell} was computed with (14),

$$T^*_{cell} = T_{cell} + \frac{\int (\dot{S}_{gen} - \dot{S}_{out})dt}{m\,Cp\,T_{cell}} \tag{14}$$

Thermal inertia is the product of the cell mass (m_{cell}) and a specific heat (Cp_{cell}). According to a review by Steinhardt et al., Cp_{cell} of cylindrical cell is between 884 J kg^{-1} K^{-1} and 1172 J kg^{-1} K^{-1}, with a lower median of 912 J kg^{-1} K^{-1} [44]. The model assumed a constant mass, m, in kg and specific heat, Cp, in J kg^{-1} K^{-1} in the cell. Assuming a constant convection coefficient, the value of h and Cp_{cell} could be computed by the least-square curve fitting of Equation (15).

$$T_{\text{cell}}(t) = T_{\text{amb}} e^{-\left(\frac{hA}{mc_p}t\right)} \tag{15}$$

The values of h and Cp_{cell} were determined experimentally by heating test samples to 50 °C and then placing them at 23 °C, while recording T_{cell} throughout the cooldown at 10 Hz until the temperature stabilized to an ambient temperature T_{amb}. Figure 7 shows the temperature of the samples during the cooldown test. A value of 31.2 W m^{-2} K^{-1} was found for h and a value of 912 J kg^{-1} K^{-1} was determined for Cp_{cell}.

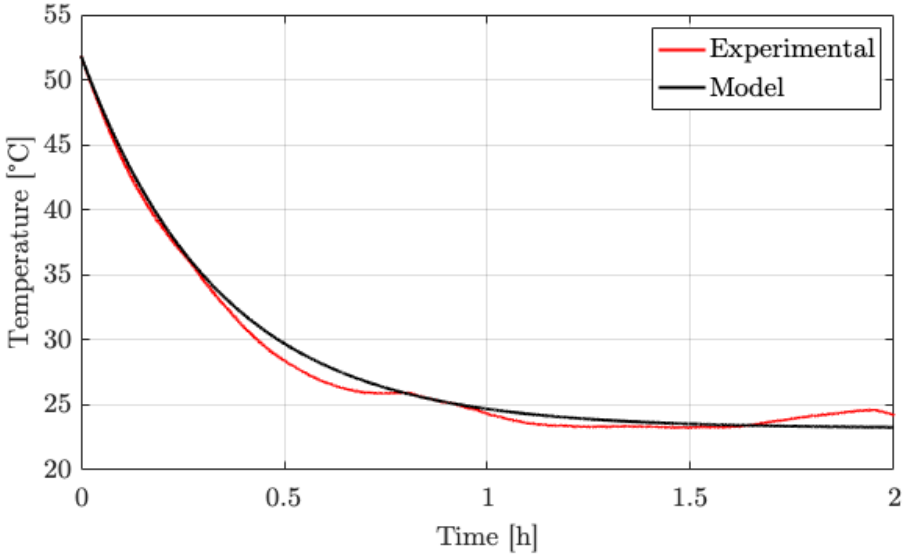


Figure 7. The cooldown of the samples from 50 °C to 23 °C compared with the model.

Other characteristics of the lithium-ion cell used in this work are gathered at Table 1.

Table 1. Cell specifications.

Name	Symbol	Value	Unit
Manufacturer	-	LG Chem	-
Model	-	INR18650MJ1	-
Chemistry	-	NMC-G	-
Nominal voltage	V_{nom}	3.65	V
Capacity	C_0	3.5	Ah
Energy	E_{nom}	12.7	Wh
Weight	m	48	g
Specific heat	Cp	912	J kg^{-1} K^{-1}
Convection	h	31.2	W m^{-2} K^{-1}

3. Results

The different parameters of the ETM were measured by a series of independent characterization procedures. The experimental validation of the model therefore had to be performed to ensure the proper implementation of the model. The validation of the model was performed using the same setup as shown in Figure 1 with a constant current discharge (1 C) and dynamic current conditions. Figure 8 shows the results of the experiment, benchmarked against the model.

The temperature in the climate chamber for this test was 23 °C. The slight fluctuations in the experimental measurement can be explained by the normal variations in temperature in the climate chamber. The results show that entropic heating mostly influenced temperature estimation. Regardless of entropic heating, the voltage error between the model and experiment was inferior to 10 mV throughout most of the discharge except below $\theta = 5\%$. Without consideration of entropic heating, the error between the model and experiment was superior to 2 °C for most of the discharge. Meanwhile, the measured error between the experimental and simulated temperatures was within 1 °C, while the overall evolution was preserved much more accurately. Thus, it can be concluded that the effect of entropy had a negligible effect on the accuracy of the electrical model but had a measurable effect on the thermal model.

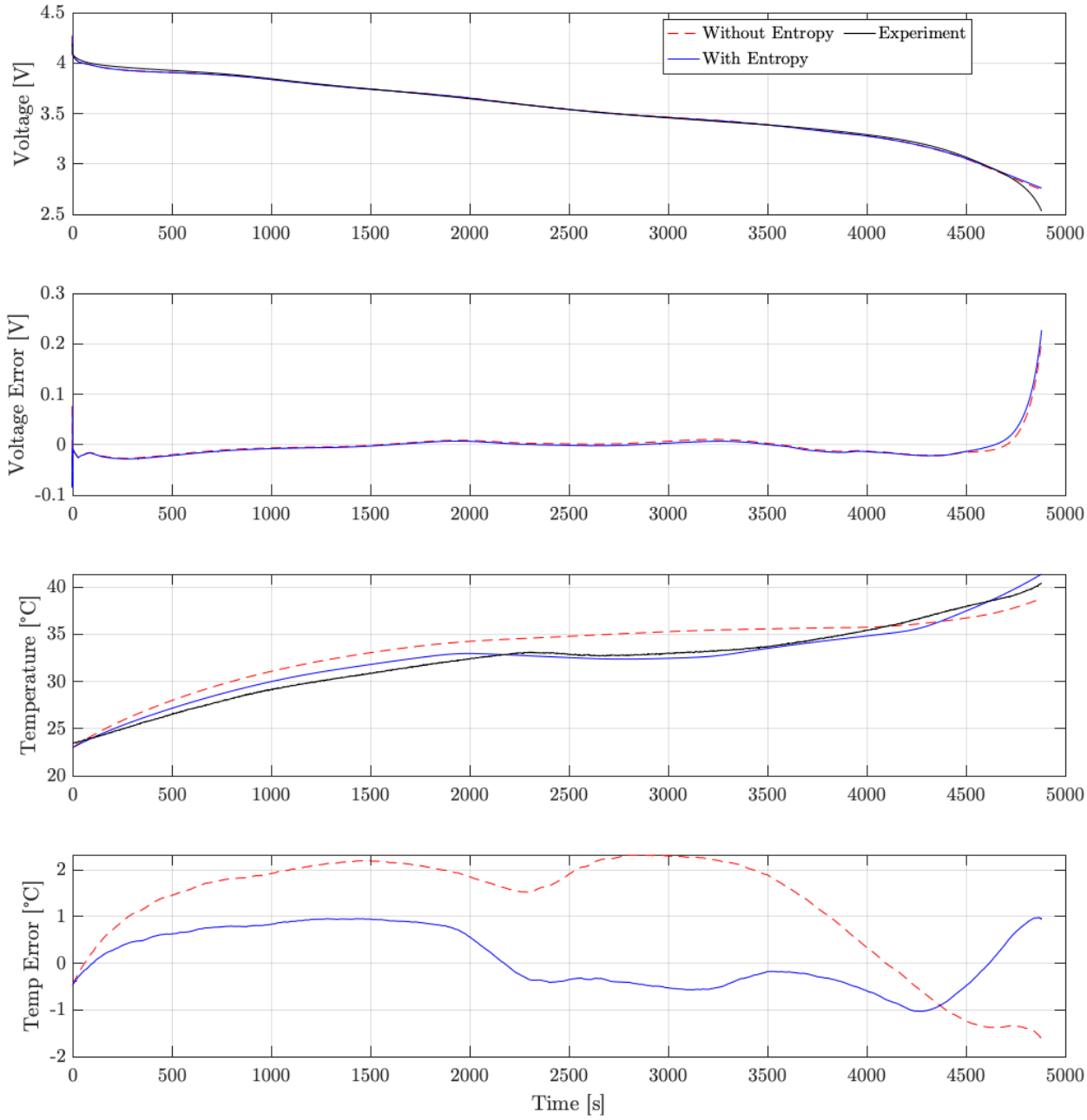


Figure 8. Constant current validation with and without entropy.

Further validation of the model was performed on a cell using a dynamic cycle from Messier et al. [45], representative of light electric vehicle drive cycle. The same experimental setup was used for this test. The vehicle current was scaled down to a cell-level equivalent current for the experiment. Figure 9 shows the applied current and the resulting voltage and temperature for the simulation and experiment.

The results show that the voltage error of the model was inferior to 70 mV throughout most of the discharge, except at θ, where it was inferior to 15%. The temperature error was inferior to 1 °C, with the highest error occurring when cell θ was between 50% and 70%, which corresponded to a rapid change in the entropic coefficient. It is likely that increasing the resolution of the entropic coefficient interpolation table could improve the thermal accuracy of the model.

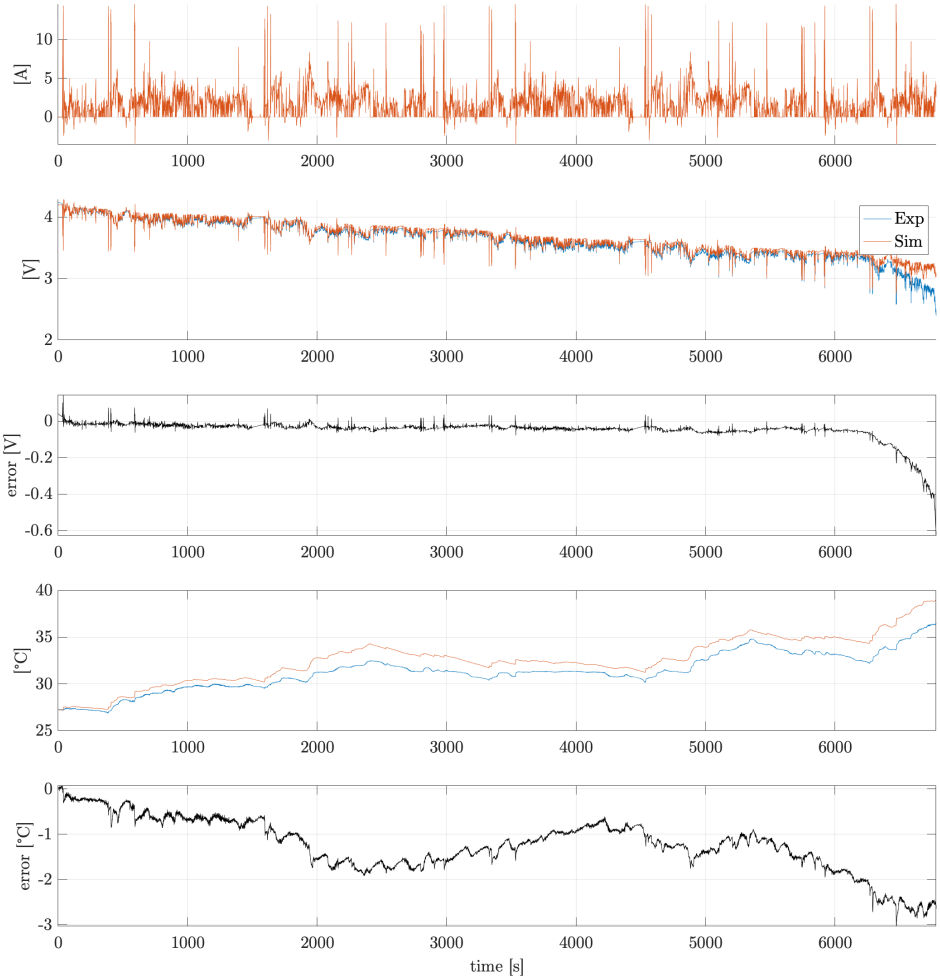


Figure 9. Electro-thermal model dynamic simulation.

4. Simulations

Having validated the model, we then explored the impact of the entropic effect in comparison with Joule losses. Though it is often stated that the entropic effect can be neglected from models since it is directly proportional to the current, it can be observed in Figures 8 and 9 that the accuracy of the thermal model was greatly improved when entropic heating was considered. To test this assumption, a constant current and constant power discharge were simulated with and without considering entropy.

4.1. Constant Current Discharge

To further our analysis, simulation results for the constant current discharge for C-rates ranging from 0.5 C to 3 C are shown in Figure 10. The results indicate that the entropic effect had a negligible effect at low discharge rates and caused a maximum error of 4 °C at higher rates. Figure 11 shows that despite the large error in heat generation seen mid-discharge, the average losses were nearly identical with and without entropy. When considering Joule losses, only the heat generation rate was much more stable, as indicated by Figure 11. Although the heat generation rate did increase at low SOCs from irreversible losses, as one would expect from the sharp increase in impedance, this rate was increased by 20% when considering entropic contribution under a constant C-rate. It is important to note here that simulation allowed us to visualize results, which would be impossible under real conditions due to the temperature limits imposed on a real lithium-ion cells because of the risks of TRA. Under real conditions, only a discharge inferior to 2 C would be acceptable.

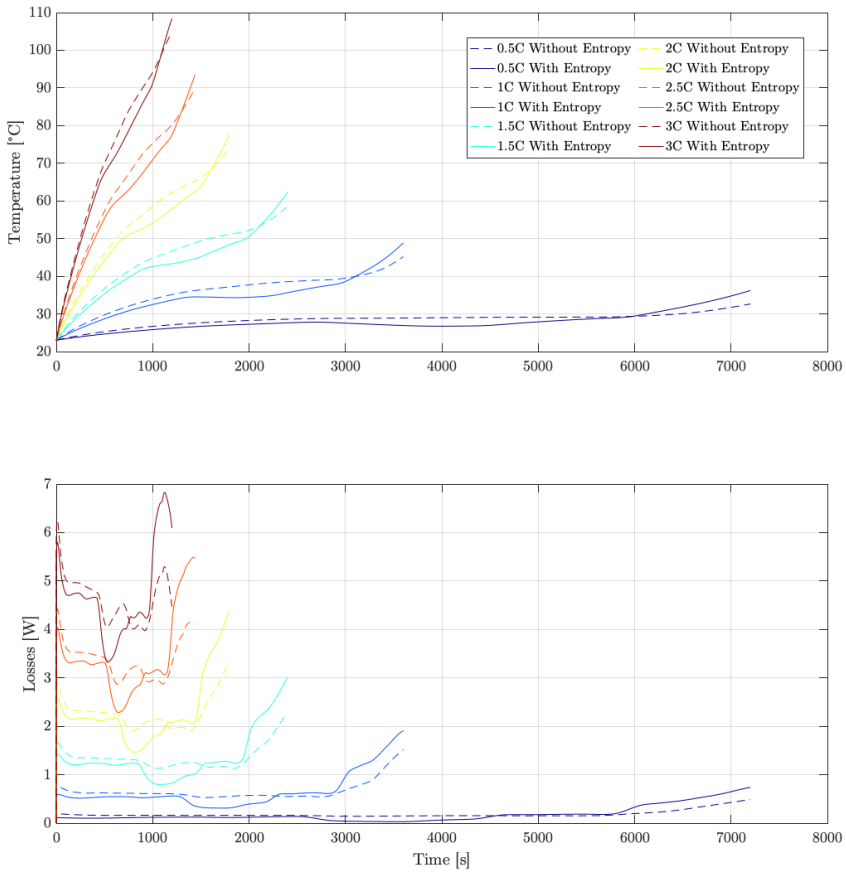


Figure 10. Constant current sensitivity analysis.

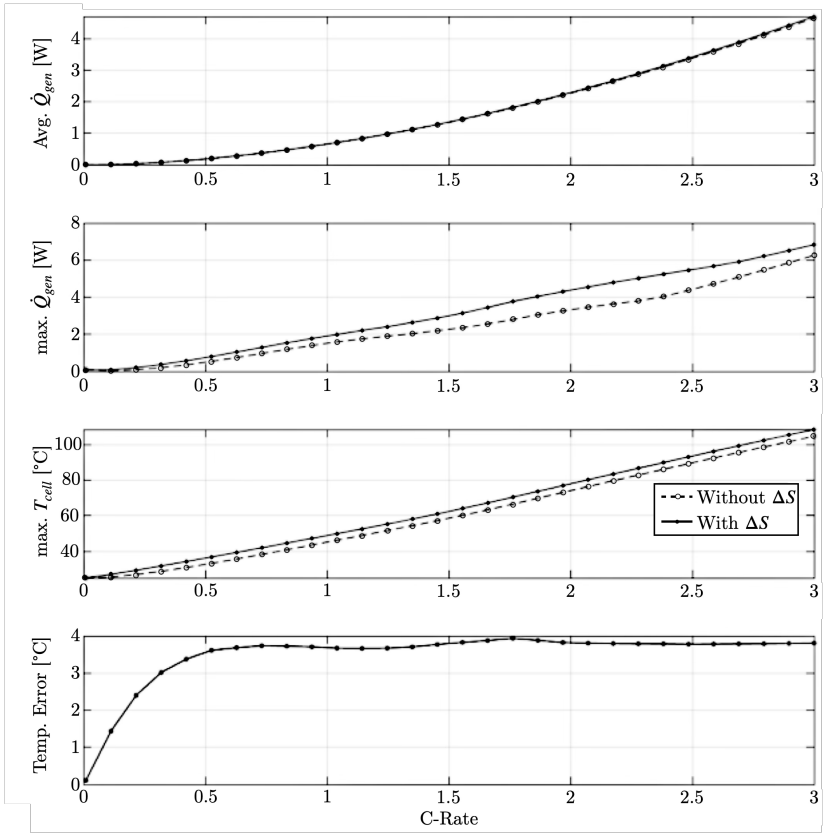


Figure 11. Sensitivity analysis of impact of C-Rate on thermal model results with and without consideration of entropic losses.

4.2. Constant Power Discharge

While galvanostatic discharge is most usual in the field of electrochemistry and the like, a constant power discharge is more representative of most engineering use cases, such as EVs. This power can be expressed in the E-rate, or multiples of the nominal energy of a cell. The nominal energy in a cell, E_{nom}, or energy storage system is equivalent to the piecewise integral of the constant current discharge curve, as stated by (16). Nominal capacity C_{nom} is defined as the total amount of charges, given in Ah, that can be stored in a cell for the electrochemical reaction to be stable.

$$E_{nom} = \int_0^{C^{nom}} V \, dC \tag{16}$$

A more practical method to estimate E_{nom} is from the product of V_{nom} and C_{nom}, typically given in product datasheets. Since V_{oc} decreases as the cell becomes depleted, the current will increase to maintain constant power. Results for discharge with constant E-rates ranging from 0.5 E to 3 E are shown in Figure 12. The boundary condition and properties were kept identical. By comparison with results of Figure 10 for a constant current discharge, the differences caused by the consideration of entropic heat generation were much less important to the proper estimation of the temperature and total heat generation. From the simulation results, it can be observed that the maximum power that could be sustained in these poor cooling conditions was 1.5 E or 19.8 W. At this E-rate, the losses could reach up to 6.5 W with entropy, while they only reached 5.3 W without entropy. This difference in heat generation was even greater at higher E-rates. As can be seen in Figure 12, Q_{gen} could reach up to 12.6 W when considering entropy. However, this specific case could not be sustained in a real application since the temperature would be significantly above the safe operational window.

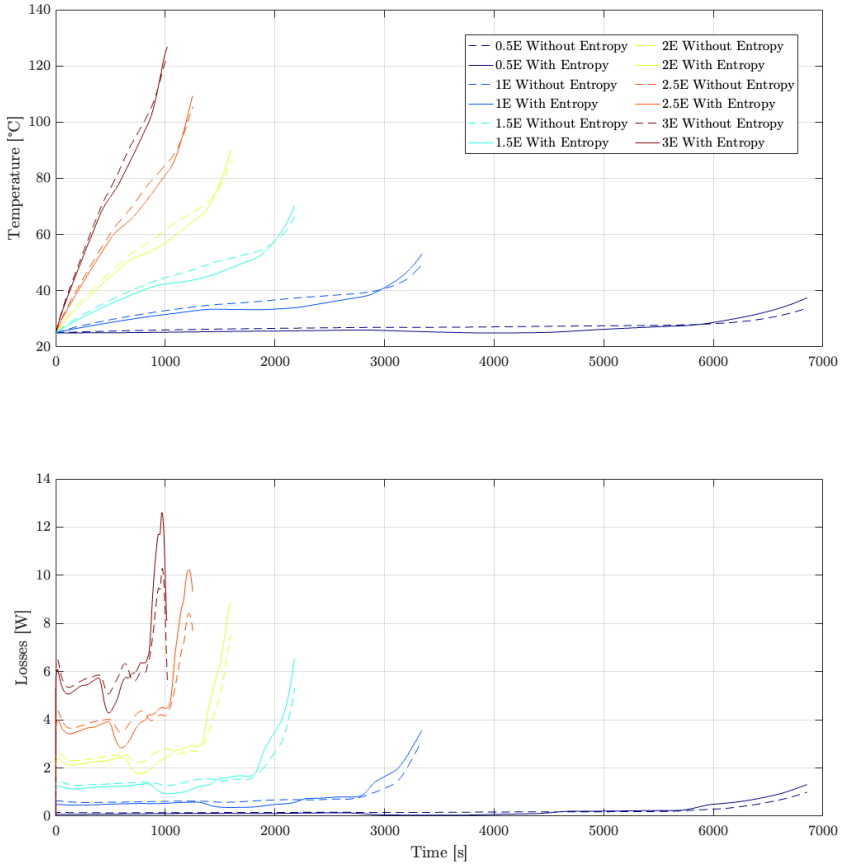


Figure 12. Constant power sensitivity analysis.

4.3. Discussion About Entropy

The estimation of heat generation is one of the primary inputs for the proper sizing of thermal management systems. Only a coarse approximation of heat generation can be made from the nominal internal resistance value. Considering the temperature and SOC dependence of internal resistance can greatly improve the accuracy of models. Further gains can be achieved by considering transient impedance instead of constant resistance. While the link between overpotentials and losses can quite easily be measured, entropy change is often overlooked due to a lack of understanding of its mechanisms. Since entropic heating is convoluted with Joule heating, it is less intuitive to measure than impedance. Simulation allowed us to deconvolute the Joule losses from entropic heating. Due to its reversibility, entropic heating cannot be considered a loss in energy per se. The exothermic phase transformation in electrodes during discharge is equally endothermic during recharge. Thus, only overpotential heating can be classified as a loss from the strict definition of losses being irreversibly lost to the environment.

The decision to consider entropy or not from thermal models can be motivated by plenty of factors. The time required to calibrate the lookup tables is one. The measurement of changes in entropy requires time, patience, well-controlled conditions, and high-precision measurement equipment. ΔS is not dependent on temperature, but it varies with SOC. Therefore, it is important to characterize this property along the entire depth of the discharge of a cell, for as many points as time allows. For instance, each data point of entropy change may take up to 1 day to obtain, simply to allow the full thermodynamic stabilization of the samples. It took 10 days to obtain the entirety of the entropic coefficient points presented in Figure 6. However, this procedure could be automated by linking the climate chamber and cell-cycler. Electro-thermal impedance spectroscopy as introduced by Schmidt et al. [46] will be considered a path to improve the speed and accuracy of the characterization of ΔS in future work.

5. Conclusions

With the increasing use of lithium-ion batteries in power-intensive applications and environments, the estimation of the thermal behaviour of lithium-ion cells through electro-thermal models becomes even more necessary to design battery packs that are safer, longer lasting, and more reliable.

This research fills a critical gap in understanding ΔS in electro-thermal modelling, offering a systematic approach to incorporating entropy change in predictive frameworks. In this work, the importance of considering ΔS in the estimation of heat generation in electro-thermal models was addressed. The electro-thermal model used for this work was structured using the energetic macroscopic representation method. The cell impedance used in the model was obtained by GITT at temperatures ranging from -20 °C to 70 °C along the entire depth of the discharge of the cells, with a resolution of a 1% SOC. The entropic coefficient was measured at increments of a 5% SOC for the entire range. A lumped thermal model with convection boundary conditions was used to estimate cell temperature.

The voltage error of the model was found to be inferior to 50 mV, while the temperature error was inferior to 1 °C when considering entropic heating, even with a dynamic drive cycle. From this validated model, sensitivity analysis was performed at various C-rates and E-rates to determine the impact of entropic heating on the temperature and total heat generation. Based on our observations, discarding entropy from the simulations could yield an error in temperature of up to 4 °C. However, the thermal boundary conditions of the present work were sub-optimal for high-power applications.

However, entropy does not seem to affect total heat generation over a full discharge. Entropy change predominantly affects the precise tracking of temperature dynamics, of-

fering critical accuracy enhancements for high-fidelity thermal simulations. It was found that it plays no significant role on the accuracy of electrical behaviour prediction. While entropy can be neglected for coarse heat generation estimation, it must be considered when temperature must be estimated with a greater level of accuracy, such as in high-fidelity thermal simulations. Future work could focus on automating entropy measurement processes and applying the findings to new chemistries or advanced thermal management systems. Incorporating entropy change into a model hinges on the desired accuracy level, available laboratory resources, and specific simulation objectives.

Author Contributions: F.-A.L.: Investigation, Methodology, Software, Validation, Writing—original draft. P.M.: Conceptualization, Validation, Writing—review and editing. M.B.: Validation, Writing—review and editing. J.P.F.T.: Resource, Conceptualization, Validation, Funding acquisition, Supervision, Writing—review and editing. All authors have read and agreed to the published version of the manuscript.

Funding: This work is supported by the Canada Research Chairs Program (950-230672) and by the Mitacs Accelerate Program under project IT30373. Authors would like to express their gratitude to SysNergie Inc. for supporting this research.

Data Availability Statement: The original contributions presented in the study are included in the article, further inquiries can be directed to the corresponding author.

Conflicts of Interest: Authors Félix-Antoine LeBel, Pascal Messier and Mathieu Blanchard were employed by the company SysNergie Inc. The remaining author declare that the research was conducted in the absence of any commercial or financial relationships that could be construed as a potential conflict of interest.

References

1. Hendricks, C.; Williard, N.; Mathew, S.; Pecht, M. A failure modes, mechanisms, and effects analysis (FMMEA) of lithium-ion batteries. *J. Power Sources* **2015**, *297*, 113–120. [CrossRef]
2. Raijmakers, L.; Danilov, D.; Eichel, R.-A.; Notten, P. A review on various temperature-indication methods for Li-ion batteries. *Appl. Energy* **2019**, *240*, 918–945. [CrossRef]
3. ouj Reynier, Y.; Yazami, R.; Fultz, B. The entropy and enthalpy of lithium intercalation into graphite. *J. Power Sources* **2003**, *119*, 850–855. [CrossRef]
4. Doyle, M.; Fuller, T.F.; Newman, J. Modeling of Galvanostatic Charge and Discharge of the Lithium/Polymer/Insertion Cell. *J. Electrochem. Soc.* **1993**, *140*, 1526. [CrossRef]
5. Fuller, T.F. Simulation and Optimization of the Dual Lithium Ion Insertion Cell. *J. Electrochem. Soc.* **1994**, *141*, 1. [CrossRef]
6. Doyle, M.; Newman, J. The use of mathematical modeling in the design of lithium/polymer battery systems. *Electrochim. Acta* **1995**, *40*, 2191–2196. [CrossRef]
7. Moura, S.J.; Argomedo, F.B.; Klein, R.; Mirtabatabaei, A.; Krstic, M. Battery State Estimation for a Single Particle Model with Electrolyte Dynamics. *IEEE Trans. Control Syst. Technol.* **2017**, *25*, 453–468. [CrossRef]
8. Erhard, S.V.; Osswald, P.J.; Wilhelm, J.; Rheinfeld, A.; Kosch, S.; Jossen, A. Simulation and Measurement of Local Potentials of Modified Commercial Cylindrical Cells. *J. Electrochem. Soc.* **2015**, *162*, A2707–A2719. [CrossRef]
9. Erhard, S.V.; Osswald, P.J.; Keil, P.; Höffer, E.; Haug, M.; Noel, A.; Wilhelm, J.; Rieger, B.; Schmidt, K.; Kosch, S.; et al. Simulation and Measurement of the Current Density Distribution in Lithium-Ion Batteries by a Multi-Tab Cell Approach. *J. Electrochem. Soc.* **2017**, *164*, A6324–A6333. [CrossRef]
10. Jokar, A.; Rajabloo, B.; Désilets, M.; Lacroix, M. Review of simplified Pseudo-two-Dimensional models of lithium-ion batteries. *J. Power Sources* **2016**, *327*, 44–55. [CrossRef]
11. Couto, L.D.; Schorsch, J.; Nicotra, M.M.; Kinnaert, M. SOC and SOH estimation for Li-ion batteries based on an equivalent hydraulic model. Part I: SOC and surface concentration estimation. In Proceedings of the 2016 American Control Conference (ACC), Boston, MA, USA, 6–8 July 2016; pp. 4022–4028. [CrossRef]
12. Couto, L.D.; Schorsch, J.; Job, N.; Léonard, A.; Kinnaert, M. State of health estimation for lithium ion batteries based on an equivalent-hydraulic model: An iron phosphate application. *J. Energy Storage* **2019**, *21*, 259–271. [CrossRef]
13. Hu, X.; Li, S.; Peng, H. A comparative study of equivalent circuit models for Li-ion batteries. *J. Power Sources* **2012**, *198*, 359–367. [CrossRef]

14. Seaman, A.; Dao, T.-S.; McPhee, J. A survey of mathematics-based equivalent-circuit and electrochemical battery models for hybrid and electric vehicle simulation. *J. Power Sources* **2014**, *256*, 410−423. [CrossRef]
15. Salda na, G.; San Martín, J.I.; Zamora, I.; Asensio, F.J.; O nederra, O. Analysis of the Current Electric Battery Models for Electric Vehicle Simulation. *Energies* **2019**, *12*, 2750. [CrossRef]
16. Wu, W.; Wang, S.; Wu, W.; Chen, K.; Hong, S.; Lai, Y. A critical review of battery thermal performance and liquid based battery thermal management. *Energy Convers. Manag.* **2019**, *182*, 262–281. [CrossRef]
17. Mousavi, G.S.M.; Nikdel, M. Various battery models for various simulation studies and applications. *Renew. Sustain. Energy Rev.* **2014**, *32*, 477–485. [CrossRef]
18. Nejad, S.; Gladwin, D.T.; Stone, D.A. A systematic review of lumped-parameter equivalent circuit models for real-time estimation of lithium-ion battery states. *J. Power Sources* **2016**, *316*, 183–196. . [CrossRef]
19. Agudelo, B.; Zamboni, W.; Monmasson, E.; Spagnuolo, G. *Identification of Battery Circuit Model from EIS Data*; HAL: Bengaluru, India, 2019.
20. Vyroubal, P.; Kazda, T. Equivalent circuit model parameters extraction for lithium ion batteries using electrochemical impedance spectroscopy. *J. Energy Storage* **2018**, *15*, 23–31. [CrossRef]
21. Nickol, A.; Schied, T.; Heubner, C.; Schneider, M.; Michaelis, A.; Bobeth, M.; Cuniberti, G. GITT Analysis of Lithium Insertion Cathodes for Determining the Lithium Diffusion Coefficient at Low Temperature: Challenges and Pitfalls. *J. Electrochem. Soc.* **2020**, *167*, 090546. [CrossRef]
22. Lebel, F.A.; Messier, P.; Sari, A.; Trovao, J.P.F. Lithium-Ion cell Equivalent Circuit Model Identification by Galvanostatic Intermittent Titration Technique. *J. Energy Storage* **2022**, *54*, 105303. [CrossRef]
23. Al Hallaj, S.; Venkatachalapathy, R.; Prakash, J.; Selman, J.R. Entropy Changes Due to Structural Transformation in the Graphite Anode and Phase Change of the $LiCoO_2$ Cathode. *J. Electrochem. Soc.* **2000**, *147*, 2432. [CrossRef]
24. Viswanathan, V.V.; Choi, D.; Wang, D.; Xu, W.; Towne, S.; Williford, R.E.; Zhang, J.G.; Liu, J.; Yang, Z. Effect of entropy change of lithium intercalation in cathodes and anodes on Li-ion battery thermal management. *J. Power Sources* **2010**, *195*, 3720–3729. [CrossRef]
25. Bazinski, S.J.; Wang, X. The Influence of Cell Temperature on the Entropic Coefficient of a Lithium Iron Phosphate (LFP) Pouch Cell. *J. Electrochem. Soc.* **2014**, *161*, A168–A175. [CrossRef]
26. MathWorks. Generic Battery Model—Simulink. 2018. Available online: https://www.mathworks.com/help/physmod/sps/powersys/ref/battery.html (accessed on 13 February 2025).
27. Ye, Y.; Shi, Y.; Cai, N.; Lee, J.; He, X. Electro-thermal modeling and experimental validation for lithium ion battery. *J. Power Sources* **2012**, *199*, 227–238. [CrossRef]
28. Quick Review: ZKETECH ZKE Battery Rack (4-Wire Kelvin AAA/AA/18650 Test Fixture). Available online: https://bit.ly/418qDso (accessed on 13 February 2025).
29. Wilson, P. Passive Components. In *The Circuit Designer's Companion*; Elsevier: Amsterdam, The Netherlands, 2017; pp. 93–157. [CrossRef]
30. CSZ MicroClimate Benchtop Test Chambers. Available online: https://www.cszindustrial.com/Products/Temperature-Humidity-Chambers/Micro-Climate-Benchtop.aspx (accessed on 13 February 2025).
31. Zilberman, I.; Ludwig, S.; Jossen, A. Cell-to-cell variation of calendar aging and reversible self-discharge in 18650 nickel-rich, silicon–graphite lithium-ion cells. *J. Energy Storage* **2019**, *26*, 100900. [CrossRef]
32. Zilberman, I.; Sturm, J.; Jossen, A. Reversible self-discharge and calendar aging of 18650 nickel-rich, silicon-graphite lithium-ion cells. *J. Power Sources* **2019**, *425*, 217–226. [CrossRef]
33. Zilberman, I.; Schmitt, J.; Ludwig, S.; Naumann, M.; Jossen, A. Simulation of voltage imbalance in large lithium-ion battery packs influenced by cell-to-cell variations and balancing systems. *J. Energy Storage* **2020**, *32*, 101828. [CrossRef]
34. Zilberman, I.; Ludwig, S.; Schiller, M.; Jossen, A. Online aging determination in lithium-ion battery module with forced temperature gradient. *J. Energy Storage* **2020**, *28*, 101170. [CrossRef]
35. Sturm, J.; Ludwig, S.; Zwirner, J.; Ramirez-Garcia, C.; Heinrich, B.; Horsche, M.F.; Jossen, A. Suitability of physicochemical models for embedded systems regarding a nickel-rich, silicon-graphite lithium-ion battery. *J. Power Sources* **2019**, *436*, 226834. [CrossRef]
36. Berg, P.; Spielbauer, M.; Tillinger, M.; Merkel, M.; Schoenfuss, M.; Bohlen, O.; Jossen, A. Durability of lithium-ion 18650 cells under random vibration load with respect to the inner cell design. *J. Energy Storage* **2020**, *31*, 101499. [CrossRef]
37. Lammer, M.; Königseder, A.; Hacker, V. Holistic methodology for characterisation of the thermally induced failure of commercially available 18650 lithium ion cells. *RSC Adv.* **2017**, *7*, 24425–24429. [CrossRef]
38. Heenan, T.M.; Jnawali, A.; Kok, M.; Tranter, T.G.; Tan, C.; Dimitrijevic, A.; Jervis, R.; Brett, D.J.; Shearing, P.R. Data for an Advanced Microstructural and Electrochemical Datasheet on 18650 Li-ion Batteries with Nickel-Rich NMC811 Cathodes and Graphite-Silicon Anodes. *Data Brief* **2020**, *32*, 106033. [CrossRef]

39. German, R.; Solis, N.; Reyes, L.; Silva, L.; LeBel, F.-A.; Trovao, J.P.; Bouscayrol, A. Coupled electric and thermal batteries models using energetic macroscopic representation (EMR) for range estimation in electric vehicles. In Proceedings of the 2017 19th European Conference on Power Electronics and Applications (EPE'17 ECCE Europe), Warsaw, Poland, 11–14 September 2017; Volume 2017, pp. 1–8. [CrossRef]
40. Barai, A.; Uddin, K.; Dubarry, M.; Somerville, L.; McGordon, A.; Jennings, P.; Bloom, I. A comparison of methodologies for the non-invasive characterisation of commercial Li-ion cells. *Prog. Energy Combust. Sci.* **2019**, *72*, 1–31. [CrossRef]
41. Beck, D.; Dechent, P.; Junker, M.; Sauer, D.U.; Dubarry, M. Inhomogeneities and Cell-to-Cell Variations in Lithium-Ion Batteries, a Review. *Energies* **2021**, *14*, 3276. [CrossRef]
42. Geifes, F.; Bolsinger, C.; Mielcarek, P.; Birke, K.P. Determination of the entropic heat coefficient in a simple electro-thermal lithium-ion cell model with pulse relaxation measurements and least squares algorithm. *J. Power Sources* **2019**, *419*, 148–154. [CrossRef]
43. Onda, K.; Kameyama, H.; Hanamoto, T.; Ito, K. Experimental Study on Heat Generation Behavior of Small Lithium-Ion Secondary Batteries. *J. Electrochem. Soc.* **2003**, *150*, A285. [CrossRef]
44. Steinhardt, M.; Barreras, J.V.; Ruan, H.; Wu, B.; Offer, G.J.; Jossen, A. Meta-analysis of experimental results for heat capacity and thermal conductivity in lithium-ion batteries: A critical review. *J. Power Sources* **2022**, *522*, 230829. [CrossRef]
45. Messier, P.; Nguyen, B.H.; LeBel, F.A. and Trovão, J.P.F. Disturbance observer-based state-of-charge estimation for Li-ion battery used in light electric vehicles. *J. Energy Storage* **2020**, *27*, 101144. [CrossRef]
46. Schmidt, J.P.; Weber, A.; Ivers-Tiffée, E. A novel and precise measuring method for the entropy of lithium-ion cells: ΔS via electrothermal impedance spectroscopy. *Electrochim. Acta* **2014**, *137*, 311–319. [CrossRef]

Disclaimer/Publisher's Note: The statements, opinions and data contained in all publications are solely those of the individual author(s) and contributor(s) and not of MDPI and/or the editor(s). MDPI and/or the editor(s) disclaim responsibility for any injury to people or property resulting from any ideas, methods, instructions or products referred to in the content.